Spin Electronics

Field and Current Driven Magnetic Domain Wall Motion in Disordered A1-FePt Nanowires

Pin Ho[1], Jinshuo Zhang[1], Jean Anne Currivan-Incorvia[1,2], David C. Bono[1], and Caroline A. Ross[1]

[1]*Department of Materials Science and Engineering, Massachusetts Institute of Technology, Cambridge, MA 02139 USA*
[2]*Department of Physics, Harvard University, Cambridge, MA 02138 USA*

Received 8 Dec 2014, revised 30 Dec 2014, accepted 10 Jan 2015, published 13 Jan 2015, current version 5 Mar 2015.

Abstract— Arc-shaped magnetic FePt nanowires (10 nm thick, 375 nm wide) displaying in-plane anisotropy were fabricated. A vortex domain wall was formed in the middle of the arc after in-plane saturation in a field perpendicular to the wire. Translational domain wall propagation was observed at a field of 40 Oe applied parallel to the wire, while complete propagation to the end of the arc occurred at 100 Oe. Domain wall displacement at low velocity was achieved by current pulses of 2.5×10^{11} A $\cdot$ m^{-2} at zero applied magnetic field, comparable to the zero-field threshold current density of Permalloy. A field-assisted spin transfer torque drove the domain wall 1.8 μm to the end of the arc.

Index Terms—Spin electronics, domain wall motion, magnetic nanowires, spin transfer torque.

I. INTRODUCTION

Domain dynamics in magnetic nanowires has attracted much attention due to its technological potential in spintronics applications [Parkin 2008]. Early work on field-induced and current-induced DW motion focused on Permalloy (NiFe) nanowires with in-plane magnetization, which display a low thin film anisotropy of typically $\sim 2 \times 10^4$ erg cm^{-3} [Yamaguchi 2004, Togawa 2006]. While an understanding of Permalloy DW dynamics has been well established, there are no reports on chemically disordered A1-structure FePt, where the larger magnetocrystalline anisotropy K_1 of magnitude 6×10^5 erg cm^{-3} promotes thermal stability against superparamagnetism [Sallica 2010]. The spin-orbit coupling and spin polarization of A1-FePt, containing non-magnetic high-Z atoms, also differ from other in-plane anisotropy films made up of magnetic transition metal alloys, and their effects on DW dynamics is an area not previously investigated. Furthermore, perpendicularly magnetized $L1_0$-FePt thin films are suitable candidates for data storage and DW based devices [Ho 2011, Ho 2011]. The A1 disordered phase is transformed into the high anisotropy $L1_0$ ordered phase by annealing. The study of A1-FePt in direct comparison to $L1_0$-FePt provides an insight into DW behavior in ordered versus disordered alloys with similar composition and electrical conductivity. Thus, an understanding of the nature of DW dynamics in disordered A1-FePt phase with in-plane anisotropy provides a useful complement to existing knowledge of DW dynamics in soft transition metal alloys and in hard $L1_0$-FePt. In this study, the DW structure, behavior and dynamics of DWs in A1-FePt nanowires under the influence of a field, pulsed current and field-assisted pulsed current were studied.

II. PREPARATION AND CHARACTERIZATION

Arc-shaped nanowires of linewidth 375 nm with 2 μm diameter injection pads [Jang 2012] were exposed on 160 nm thick polymethyl methacrylate resist spin coated on a naturally oxidized Si (100) substrate, using a Raith 150 electron beam lithography tool. FePt (10 nm thick) was subsequently ion beam sputtered at room temperature from a $Fe_{55}Pt_{45}$ target on patterned resist-coated Si/SiO_2 substrate, with Ar pressure of 1.5×10^{-4} Torr and base pressure better than 8×10^{-7} Torr. The FePt deposition rate was 0.033 nm s^{-1} with an Ar ion gun discharge current, beam current, and beam voltage of 0.9 A, 50 mA, and 1000 V, respectively. A composition of $Fe_{57}Pt_{43}$ was determined from energy dispersive spectroscopy analysis. Top electrodes of Au (130 nm)/Ta (7 nm) were also patterned on the nanowire for the injection of current pulse and electrical measurements (see Fig. 1). The nanowires and Au electrode pads were imaged with a scanning electron microscope in the Raith 150.

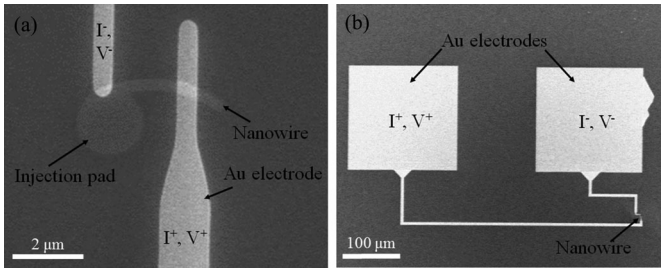

Fig. 1. Scanning electron microscopy image showing (a) Au conduction electrode pads on the arc-shaped nanowire for the injection of current pulses and electrical measurements. (b) Overview of the features at a lower magnification.

Magnetic properties of unpatterned FePt thin films were characterized by an ADE model 1660 vibrating sample magnetometer (VSM). Lattice spacing and crystal orientation were studied using X-ray diffraction (XRD) on a PANalytical multipurpose diffractometer with Cu K_α radiation. Feature dimensions were measured using a Veeco Nanoscope IV atomic force microscope (AFM). AFM showed that thin side walls of $\sim$10 nm height were present in some regions of the nanowire edges. The magnetic domain structures in the wires were mapped out

Corresponding author: P. Ho (hopin@mit.edu).
Digital Object Identifier 10.1109/LMAG.2015.2392079

with magnetic force microscopy (MFM, Veeco Nanoscope IV) using a low moment CoPtCr tip to minimize the influence of stray field on the DWs in the wires. Repeated imaging of the same sample did not show any tip-induced contrast changes suggesting that the tip did not significantly disturb the wall.

Simulations were performed with the 3-D OOMMF micromagnetic solver [Donahue 1999] for 2 μm long, 60–420 nm wide, and 10 nm thick FePt nanowires with a random uniaxial anisotropy, saturation magnetization, and exchange constant of 5×10^5 erg $\cdot$ cm^{-3}, 1000 emu $\cdot$ cm^{-3}, and 1×10^{-6} erg $\cdot$ cm^{-1}, respectively. Both transverse and vortex walls were initiated in the wires then relaxed, and the state with lower energy was taken as the stable DW structure.

The unpatterned disordered A1-FePt thin film with a characteristic (111) XRD peak demonstrated an in-plane easy axis. The FePt film had a low root mean square surface roughness of 0.7 nm and displayed an in-plane coercivity of 80 Oe and saturation magnetization M_s of 1000 $\pm$ 50 emu $\cdot$ cm^{-3}. The out-of-plane magnetization did not saturate at 10 kOe, but its magnetization at that field was close to the in-plane saturation value, suggesting an anisotropy field slightly above 10 kOe. This is consistent with the dominant anisotropy originating from the demagnetization field ($4\pi\ M_s$), although it is possible that smaller magnetocrystalline or magnetoelastic contributions to the net anisotropy are present.

III. DOMAIN WALL MOTION

The FePt nanowire was initially saturated in $H_y = 10$ kOe transverse to the midpoint of the wire. Upon the removal of the field, a 180° DW was introduced from the injection pad into the wire [Fig. 2(a)]. The DW was present in the midpoint of the arc upon remanence, evident from the bright yellow contrast in the MFM image. The image was characteristic of a vortex wall, rather than a transverse DW, showing a vortex with a darker core. The existence of a vortex wall is consistent with micromagnetic simulations, which affirmed the lower energy of vortex walls at a nanowire width greater than 100 nm [see Fig. 2(d)].

At an applied field of $H_x = 20$ Oe parallel to the FePt nanowire, the DW remained pinned. However, at a larger applied field in the range of 40–80 Oe, there was small translational propagation of the DW [see Fig. 2(b)]. There was no visible change in the DW structure after this field-driven DW motion, according to MFM. The limited movement of the DW is attributed to the existence of pinning sites and the deviation of the wire direction from the direction of H_x. At an applied field of $H_x = 100$ Oe, the bright contrast of the DW was no longer visible near the arc center and the dark contrast at the end of the wire reversed. This shows that the DW propagated to the end of the arc and was eliminated [see Fig. 2(c)].

Current driven DW motion was investigated in the arc-shaped nanowire by passing a pulsed current through the Au electrode pads and nanowire. For the highest voltage (8 V) and current density, the DW position was measured by MFM after applying each 10 μs current pulse without resetting the DW position. For lower current densities, a series of 50 or more current pulses

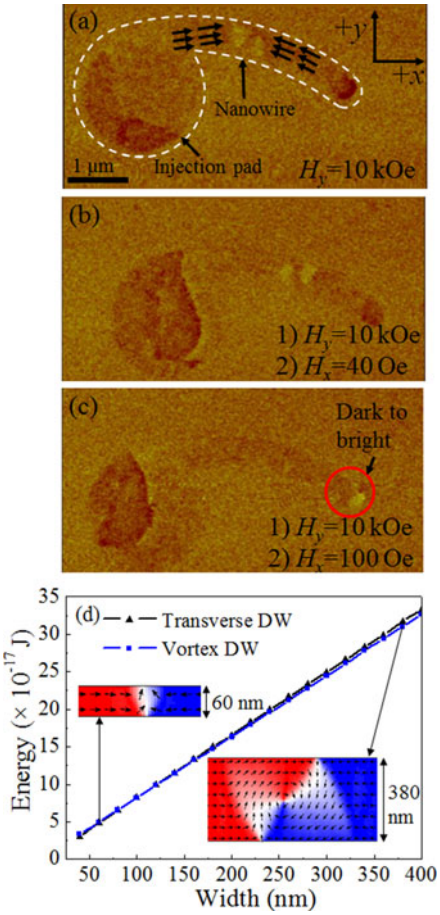

Fig. 2. 6×3 μm MFM images of the nanowire illustrating DW propagation under the influence of an applied field H_x parallel to the nanowire with magnitude of (a) 0, (b) 40, and (c) 100 Oe upon remanence. Arrows in nanowire of (a) indicate direction of magnetization in the wire. In (c), the end of the wire reversed its contrast. (d) Energies of transverse and vortex DW in a 2000 nm long, 10 nm thick A1-FePt nanowire with different widths from OOMMF simulations. The vortex wall is lower energy for nanowire widths greater than 100 nm.

was applied, the DW position was measured by MFM, then the DW position was reset by saturating the nanowire with $H_y = 10$ kOe, and a further sequence of pulses was applied. The position of the DW was determined with respect to a reference point located at the intersection of the nanowire arc and circular injection pad, indicated by the blue arrows in Fig. 3. The DW position is recorded as the edge of the wall nearest to the reference point, labeled by the black arrows in the MFM images. For the low current density experiments, each reset may produce a slightly different initial position of the DW because the orientation of the field may have differed by a few degrees. To account for this, the position of the wall in a control sample [see Fig. 3(a)–(c)] was used as an internal reference, and the amount of current-driven displacement was obtained by comparing the position of the wall in the current-pulsed sample [Fig. 3(d)–(f)] with that in the reference [Fig. 3(a)–(c)]. The reference nanowire was patterned on the same SiO_2 substrate in close proximity to the electrically contacted nanowire. The use of a reference also allowed the effects of a simultaneous field and current to be separated.

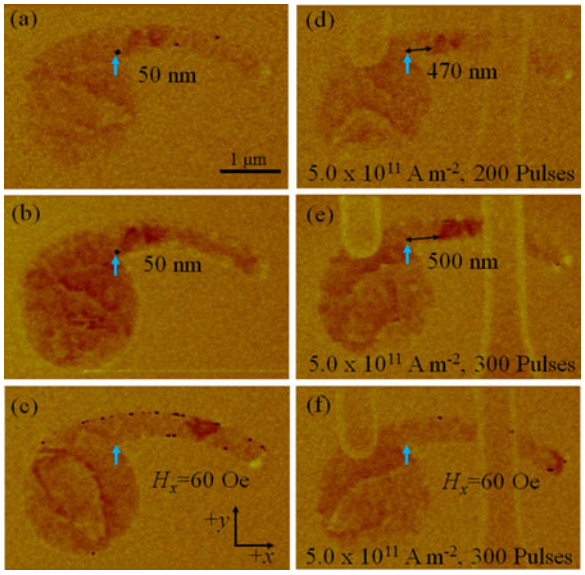

Fig. 3. $4.5 \times 3\ \mu$m MFM images of arc-shaped FePt nanowires. (a) and (b) are controls indicating the initial position of the DW after remanence, and (c) is a control indicating the position of the DW after $H_x = 60$ Oe transverse field was applied. (d) and (e) indicate the position of the DW after the injection of different numbers of current pulses, and (f) indicates the DW position after the application of field and current.

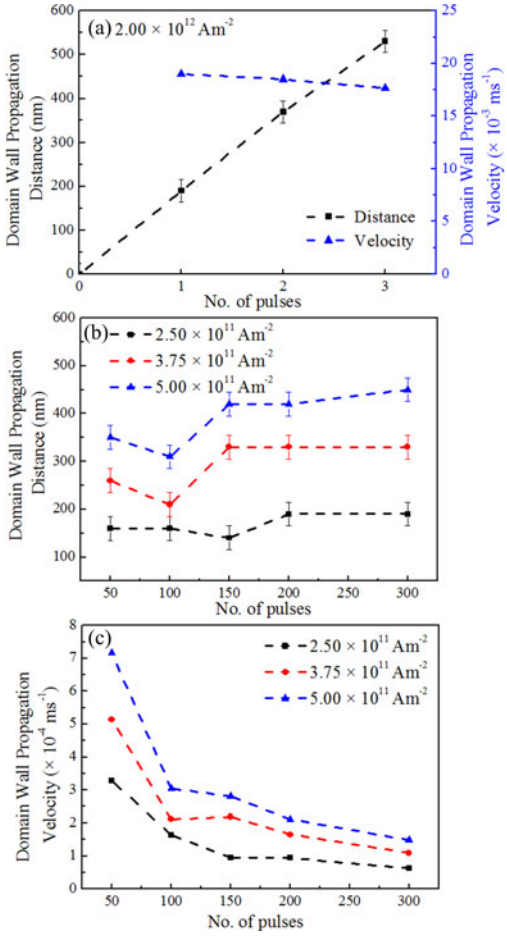

Fig. 4. (a) Displacement and velocity of the FePt DW at a current density of 2.0×10^{12} A · m^{-2} (b) Displacement and (c) velocity of the DW in the FePt nanowires with respect to the number of current pulses injected for current densities of 2.5×10^{11}, 3.75×10^{11}, and 5.0×10^{11} A · m^{-2}. Error bar for the displacement in (a) and (b) is the estimated MFM resolution. The dashed lines serve as a guide for the eye.

We first describe current-driven DW motion under the influence of a large 8 V pulse voltage. Given that the combined resistance of the circuit including the nanowire was $1000 \pm 50\ \Omega$ and the cross-sectional area of the nanowire was approximately 10×375 nm^2, a current of 8 mA and current density of 2.0×10^{12} A · m^{-2} in the FePt wire was obtained. The Au electrode of width 540 nm and thickness 130 nm carried a current density of 1.1×10^{11} A · m^{-2}. Treating the rectangular Au electrode as four adjacent circular wires of diameter 130 nm each carrying 2 mA current, the Biot–Savart Law estimates a field of 19 Oe at the position of initial A1-FePt DW 600 nm away from the edge of the rectangular Au electrode. This field is oriented out-of-plane and is smaller in magnitude than the 40 Oe in-plane field required to drive DW motion, and thus, its influence on the initial DW velocity is neglected. Fig. 4(a) shows a linear increase in DW displacement with each additional current pulse injected. The average velocity of the DW was calculated by dividing the DW displacement over the total duration of pulse injection. Each current pulse of 2.0×10^{12} A · m^{-2} drove the DW an average distance of 184 nm, at a velocity of 0.0184 m · s^{-1}.

This current density produced clearly measurable DW displacement, but also led to Joule heating of the sample which could promote thermally activated DW depinning and affect the DW velocity. To minimize the effect of Joule heating, subsequent studies of current-induced DW motion were carried out at lower current densities of $2.5–5 \times 10^{11}$ A · m^{-2}, and a larger number of pulses was employed to generate sufficient DW displacement to be detected by MFM. To estimate the temperature rise for a current density of 5×10^{11} A · m^{-2}, the resistance of the FePt nanowire was compared before pulsing and 10 to 200 ms after the end of 50 to 300 pulse injections. Pulses were 10 μs long with 1 s intervals. Taking a FePt thermal coefficient of resistivity of 3×10^{-3} K^{-1} [Giancoli 1995], the temperature change T (K) versus cooling time t (ms) was calculated. The temperature rise was 3.0 and 0.5 K at 10 and 200 ms, respectively, after the end of the 5×10^{11} A · m^{-2} pulse. There was no dependence of temperature on the number of pulses indicating that the sample had enough time to cool after each pulse. The T (K) versus t (ms) plot was fitted with an exponential decay of heat with time, $T(t) \propto \exp\left(-\frac{t}{\tau}\right)$, where τ was fitted to a value of 120 ms. The extrapolation of the graph estimates a temperature increase of 3.3 K at $t = 0$, immediately after the current was turned off.

In addition, the expected temperature change was also calculated from the heat conduction expression of [You 2006]. A temperature rise of up to 25 K was estimated for a 10 μs pulse of 5×10^{11} A · m^{-2}, based on the A1-FePt electrical conductivity of $5.6 \times 10^5\ \Omega^{-1} \cdot$ m^{-1} (resistance: 850 Ω, wire length between Au electrodes: 1.8 μm, cross-sectional area: 10×375 nm^2), Si substrate thermal diffusivity of 8.6×10^5

$m^2 \cdot s^{-1}$ [Yoo 2002], Si volumetric heat capacity of 1.6×10^6 $J \cdot m^{-3}$ K^{-1} [Yoo 2002], and assuming a Gaussian profile parameter of 0.5. The two methods suggest that the temperature rise from Joule heating is modest for current pulsing of 5×10^{11} $A \cdot m^{-2}$.

Fig. 3(d) and (e) show the DW positions after applying a current density of 5×10^{11} $A \cdot m^{-2}$ with pulse duration of 10 μs and interval between pulses of 1 s, consisting of 200 and 300 pulses, respectively. The FePt DW propagated away from the circular injection pad in the direction of electron flow. Reversing the current direction, the DW propagated in the opposite direction toward the injection pad (not shown). This observed symmetry indicates that DW motion is driven by spin transfer torque. DW displacement due to spin transfer torque was also observed at 2.5×10^{11} $A \cdot m^{-2}$. This current density for the A1-FePt DW zero-field motion falls in the same range as the zero-field threshold current density of $1.9–12 \times 10^{11}$ $A \cdot m^{-2}$ for Permalloy [Yamaguchi 2004, Togawa 2006]. Using reported values of $L1_0$-FePt spin polarization factor, A1-FePt Gilbert damping constant and $L1_0$-FePt nonadiabatic spin torque parameter of 0.4 [Seki 2008], 0.028 [Chen 2012], and 0.06 [Burrowes 2009], respectively, OOMMF simulations predicted a threshold spin current density of 2.15×10^{11} $A \cdot m^{-2}$ for FePt DW motion in a 380 nm wide, 10 nm thick wire without extrinsic pinning sites or roughness. The modeling is limited by the omission of pinning and by the uncertainty in the spin polarization and nonadiabatic parameter for A1-FePt, but despite this, the predicted threshold current density was similar to that seen experimentally.

The propagation distance of the FePt DW due to current pulses of $2.5–5 \times 10^{11}$ $A \cdot m^{-2}$ is summarized in Fig. 4(b). At 5×10^{11} $A \cdot m^{-2}$, the wall displacement increased then saturated with increasing number of current pulses. With larger number of current pulses, the wall moved far enough that its leading edge reached the second contact pad. At this location, the current is shunted by the gold pad, and the spin current density in the nanowire decreased, which impeded DW propagation [Jang 2012]. For lower current densities, the DW propagated a shorter distance, and we speculate that the wall became pinned, and the spin current density was insufficient to depin it.

The FePt DW propagated with an average velocity in the range of $3–7 \times 10^{-4}$ $m \cdot s^{-1}$ during the first 50 pulses at $2.5–5 \times 10^{11}$ $A \cdot m^{-2}$ [see Fig. 4(c)], which was significantly slower than the velocity of 3 $m \cdot s^{-1}$ reported for Permalloy using a current density of 1.2×10^{12} $A \cdot m^{-2}$ [Yamaguchi 2004]. Even at 2×10^{12} $A \cdot m^{-2}$, the FePt DW velocity was only 0.0184 m s^{-1} [see Fig. 4(a)]. The low velocity is attributed to poorer polarization and spin transfer efficiency in FePt, a result of strong spin orbit scattering by the Pt atoms in the alloy [Kent 2010].

Field-assisted current-induced DW motion was using applied field in the range of $H_x = 20$ to 60 Oe and 300 pulses of 5.0×10^{11} $A \cdot m^{-2}$ current. There was no DW motion in the nanowire with an applied field $H_x = 20$ Oe but a combination of both $H_x = 20$ Oe and 5.0×10^{11} $A \cdot m^{-2}$ current drove the DW a distance of 610 nm, propagating further than the distance of 450 nm obtained after 300 pulses of current density 5.0×10^{11} $A \cdot m^{-2}$ alone. Fig. 3(c) and (f) demonstrate field-assisted current-induced DWM, where 5.0×10^{11} $A \cdot m^{-2}$ current and a field of $H_x = 60$ Oe were applied concurrently. The field-assisted current pulse drove the DW to the end of the arc, traveling at least 1.8 μm away from the center of the arc and passing under the electrode. The combined use of field and current provided sufficient driving force on the wall to overcome threshold and pinning effects. Thus, in the presence of $H_x = 60$ Oe external field, a relatively low pulsed current density was able to bring about significant DW displacement in the arc-shaped FePt thin film.

ACKNOWLEDGMENT

This work was supported by the Agency of Science, Technology and Research (A*STAR) International Fellowship Grant, the National Science Foundation, and C-SPIN, one of six STARnet Centers of SRC supported by DARPA and MARCO. The authors would like to thank G. S. Beach, M. Mann, and L. Caretta of MIT for experimental advice.

REFERENCES

Burrowes C, Mihai A P, Ravelosona D, Kim J-V, Chappert C, Vila L, Marty A, Samson Y, Garcia-Sanchez F, Buda-Prejbeanu L D, Tudosa I, Fullerton E E, Attane J-P (2010), "Non-adiabatic spin-torques in narrow magnetic domain walls," *Nat. Phys.*, vol. 6, pp. 17–21, doi: 10.1038/nphys1436.

Chen Z, Yi M, Chen M, Li S, Zhou S, Lai T (2012), "Spin waves and small intrinsic damping in an in-plane magnetized FePt film," *Appl. Phys. Lett.*, vol. 101, 222402, doi: 10.1063/1.4768787.

Donahue M, Porter D (1999), *OOMMF User's Guide: Version 1.0*, National Institute of Standards and Technology, Gaithersburg, MD, USA.

Giancoli D C (1995), *Physics: Principles With Applications*, 4th ed. Englewood Cliffs, NJ, USA: Prentice-Hall.

Ho P, Han G C, Evans R F L, Chantrell R W, Chow G M, Chen J S (2011), "Perpendicular anisotropy $L1_0$-FePt based pseudo spin valve with Ag spacer layer," *Appl. Phys. Lett.*, vol. 98, 132501, doi: 10.1063/1.3571450.

Ho P, Han G C, He K H, Chow G M, Chen J S (2011), "(001) textured $L1_0$-FePt pseudo spin valve with TiN spacer," *Appl. Phys. Lett.*, vol. 99, 252503, doi: 10.1063/1.3671988.

Jang Y, Bowden S R, Mascaro M, Unguris J, Ross C A (2012), "Formation and structure of 360 and 540 degree domain walls in thin magnetic stripes," *Appl. Phys. Lett.*, vol. 100, 062407, doi: 10.1063/1.3681800.

Jang Y, Mascaro M D, Beach G S D, Ross C A (2012), "Current-driven domain wall motion in heterostructured ferromagnetic nanowires," *Appl. Phys. Lett.*, vol. 100, 112401, doi: 10.1063/1.3692797.

Kent A D (2010), "Spintronics: Perpendicular all the way," *Nat. Mater.*, vol. 9, pp. 699–700, doi: 10.1038/nmat2844.

Parkin S S P, Hayashi M, Thomas L (2008), "Magnetic domain-wall racetrack memory," *Science*, vol. 320, pp. 190–194, doi: 10.1126/science.1145799.

Sallica L E, Valente R C, Martínez T F, Vásquez M M, Roshdestwensky S, Butera A (2010), "Magnetic domain crossover in FePt thin films," *Phys. Rev. B.*, vol. 82, 144410, doi: 10.1103/PhysRevB.82.144410.

Seki T, Hasegawa Y, Mitani S, Takahashi S, Imamura H, Maekawa S, Nitta J, Takanashi K (2008), "Giant spin Hall effect in perpendicularly spin-polarized FePt/Au devices," *Nat. Mater.*, vol. 7, pp. 125–129, doi: 10.1038/nmat2098.

Togawa Y, Kimurai T, Harada K, Akashi T, Matsuda T, Tonomura A, Otani Y (2006), "Domain nucleation and annihilation in uniformly magnetized state under current pulses in narrow ferromagnetic wires," *Jpn. J. Appl. Phys.*, vol. 45, pp. L1322–L1324, doi: 10.1143/JJAP.45.L1322.

Yamaguchi A, Ono T, Nasu S, Miyake K, Mibu K, Shinjo T (2004), "Real-space observation of current-driven domain wall motion in submicron magnetic wires," *Phys. Rev. Lett.*, vol. 92, 077205, doi: 10.1103/PhysRevLett.92.077205.

Yoo W S, Fukada T, Yokoyama I, Kang K, Takahashi N (2002), "Thermal behavior of large-diameter silicon wafers during high-temperature rapid thermal processing in single wafer furnace," *Jpn. J. Appl. Phys.*, vol. 41, pp. 4441–4449, doi: 10.1143/JJAP.41.4442.

You C-Y, Sung I M, Joe B-K (2006), "Analytic expression for the temperature of the current-heated nanowire for the current-induced domain wall motion," *Appl. Phys. Lett.*, vol. 89, 222513, doi: 10.1063/1.2399441.